0-π qubit with one Josephson junction

Guo-Liang Guo [1,2] Han-Bing Leng,[1,2] Yong Hu,[1] and Xin Liu [1,2,*]

[1]*School of Physics and Institute for Quantum Science and Engineering, Huazhong University of Science and Technology,
Wuhan, Hubei 430074, China*

[2]*Wuhan National High Magnetic Field Center and Hubei Key Laboratory of Gravitation and Quantum Physics,
Wuhan, Hubei 430074, China*

Quantum states are usually fragile, making quantum computation less stable than classical computation. Quantum correction codes can protect quantum states but need many physical qubits to encode a single logical qubit. Alternatively, protecting quantum states at the hardware level has been recently developed to maintain the coherence of the quantum information by using symmetry. However, it generally has to pay the expense of increasing the complexity of the quantum devices. In this work, we propose to approach the protection of quantum states at the hardware level without increasing the complexity of the devices. The interplay between the spin-orbit coupling and the Zeeman splitting in the semiconductor allows us to tune the Josephson coupling in terms of the spin degree of freedom of Cooper pairs, the hallmark of the superconducting spintronics. This leads to the implementation of the parity-protected 0-π superconducting qubit with only one highly transparent superconductor-semiconductor Josephson junction, which makes our proposal immune from the various fabrication imperfections.

Superconducting circuits provide a promising platform for quantum computing [1–4]. They utilize the Josephson effect [5,6], the coherent tunneling of Cooper pairs, to obtain the necessary anharmonicity to form superconducting qubits [7]. Therefore, the Josephson junction is the core unit of superconducting quantum computation. At present, a superconducting qubit based on the transmon [8] has achieved high fidelity in both single-qubit and two-qubit gates [9–12]. However, since its junction is composed of an insulator, the manipulation of the Josephson junction is limited to only one degree of freedom after fabrication, the Josephson coupling energy. This makes it difficult to balance the contradictory requirements for enhancing the anharmonicity and reducing the charge noise. For transmon-like qubits, a small anharmonicity is an inevitable compromise to suppress the charge noise, although it will result in unwanted excitation to high-level states. The recently developed 0-π qubit [13,14] has a great potential to solve this contradiction while protecting the quantum coherence at the hardware level [15–18]. As the implementation of 0-π qubit requires an additional controllable degree of freedom [19–22], for the transmon-like qubit, the price paid is to increase the complexity of the circuit [23]. On the other hand, the Josephson effect has achieved tremendous progress over the past two decades, which is mainly due to the replacement of junction materials with semiconductors [24–29], ferromagnets [30–35], topological insulators [36–45], etc. These studies not only improve the tunability of the Josephson coupling energy but also enable the multidimensional control of the Josephson junction [46–53]. The former has given birth to gatemon qubits [54–62], which is based on the same principle

as the transmon but with fully electrical control, and is leading to more transmon variants. The latter not only has spawned the field of superconducting spintronics [63] but also is benefiting many other fields such as topological quantum computing [64,65].

In this work, we propose to implement the 0-π qubit with only one Josephson junction [Fig. 1(a)], utilizing the Cooper pairs' spin degrees of freedom. The spin splitting in the semiconductor region provides two Fermi surfaces, which effectively form two Josephson junctions with almost identical Josephson coupling energy. This identity is robust against various fabrication and control imperfections such as gate voltage fluctuations and disorders. The interplay among the spin-orbit coupling, Zeeman effect, and superconductivity induces the spin-singlet and spin-triplet Cooper pairs' transition through the quantum interference between the two Fermi surfaces. This interplay can suppress the single Cooper pair tunneling and realize the degenerated 0-π qubit states when the junction region only supports a few transverse modes. A gatemon-like qubit is an ideal platform to realize this proposal. Finally, with the practical experimental parameters, we show that the qubit relaxation time T_1 and coherent time T_2 can be dramatically increased, exhibiting the advantages in superconductor-semiconductor (SC-Sm) based qubits.

Josephson potential. The Josephson potential generally takes the form [66]

$$V_J(\hat{\phi}) = \sum_m E_{J\alpha}^{(m)} \cos(m\hat{\phi}) + E_{J\beta}^{(m)} \sin(m\hat{\phi}), \tag{1}$$

with $\hat{\phi}$ the superconducting phase operator. The $\sin(m\hat{\phi})$ term in Eq. (1) is allowed when the system breaks both time-reversal and inversion symmetries. In the
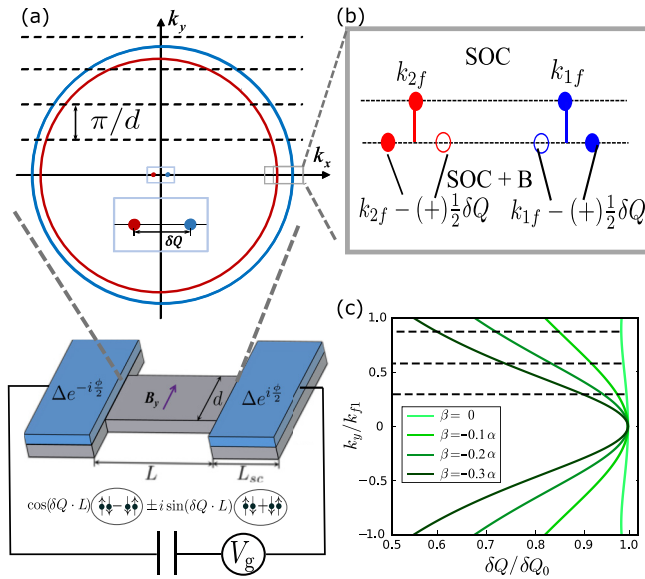
FIG. 1. (a) The setup of a SC/Sm/SC Josephson junction with a few transverse channels. The red and blue circles indicate the Fermi surfaces with opposite chirality due to the Rashba SOC. δQ_0 is the shift for $k_y = 0$ channel. (b) The momenta of electron and hole at the Fermi surface with only SOC (line above) and with both SOC and magnetic field (line below). k_{1f} and k_{2f} are the Fermi wave vectors with only SOC. Solid and hollow circles represent electron and hole; red and blue represent inner and outer Fermi surfaces as in (a). (c) The shift of the Fermi surfaces (normalized by δQ_0) as a function of the momentum k_y with the ratio $\beta/\alpha =$ 0, 0.1, 0.2, 0.3.

superconductor/insulator/superconductor junction, the Josephson effect is completely dominated by the single Cooper pair tunneling, corresponding to the Josephson potential $E_{J\alpha}^{(1)} \cos \hat{\phi}$. Replacing the insulator with semiconductors or metals increases the transparency of the Josephson junction that enhances the tunneling of multiple Cooper pairs, corresponding to $m > 1$ Josephson potentials [57]. Here, we consider the normal region as the semiconductor whose Hamiltonian takes

$$H_{\text{sm}} = \frac{\hbar^2 k^2}{2m^*} \sigma_0 + \boldsymbol{h}(\boldsymbol{k}) \cdot \boldsymbol{\sigma} + M(x)\sigma_y,$$

with m^* the effective mass, $\boldsymbol{h}$ the spin-orbit coupling (SOC) field, $M = g\mu_B B$ the Zeeman field strength, g the effective g-factor, μ_B the Bohr magneton, and B the magnetic field along y direction. The SOC Hamiltonian in a semiconductor such as InSb two-dimensional electron gas takes the form

$$\boldsymbol{h}(\boldsymbol{k}) \cdot \boldsymbol{\sigma} = (\alpha + \beta)k_x \sigma_y - (\alpha - \beta)k_y \sigma_x, \quad (2)$$

with α (β) the Rashba (Dresselhaus) SOC strength and k_x parallel with the [110] direction of InSb [67]. Without magnetic field and only taking the Rashba SOC, the electrons split into two Fermi surfaces as

$$E_{\pm} = \frac{\hbar^2 k^2}{2m^*} \pm \alpha k, \quad (3)$$

where $+$ $(-)$ corresponds to the smaller (larger) Fermi surface with Fermi wave vector k_{2f} (k_{1f}) [Fig. 1(a)]. Each Fermi

surface can independently support Cooper pairs with zero center-of-mass momentum. Adding an external magnetic field along the y direction, the two Fermi surfaces are shifted oppositely in the x direction [Figs. 1(a) and 1(b)], resulting in opposite center-of-mass momentum of the Cooper pairs supported by each Fermi surface [68–70]. In the limit of $M \ll |h(k_f)| \ll E_f$ and $\beta = 0$ with $k_f = (k_{1f} + k_{2f})/2$, the center-of-mass momentum satisfies $|\delta Q| \approx 2M/\hbar v_f$ in almost all k_y channels. When the Cooper pairs enter the normal region, they will be split into two Fermi surfaces and gain opposite center-of-mass momentum as $e^{i\delta Q \cdot x} |\uparrow\downarrow\rangle$ and $e^{-i\delta Q \cdot x} |\downarrow\uparrow\rangle$ [Fig. 1(a)]. Superposing the Cooper pairs with the opposite center-of-mass momentum leads to the oscillation of the spin singlet and spin triplet,

$$\cos(\delta Q \cdot x)(|\uparrow\downarrow\rangle - |\downarrow\uparrow\rangle) + i \sin(\delta Q \cdot x)(|\uparrow\downarrow\rangle + |\downarrow\uparrow\rangle)$$
$$= \cos(\delta Q \cdot x)|S = 0\rangle + i \sin(\delta Q \cdot x)|S = 1, S_z = 0\rangle, \quad (4)$$

where S and S_z are the total spin angular momentum and its z component. With $\delta Q \cdot L = \pi/2$, if the spin-singlet Cooper pair is injected at the SC/Sm interface ($x = 0$), it will be fully converted to spin-triplet pairs at the Sm/SC interface ($x = L$) as shown in Fig. 1(a). As the s-wave superconductor only allows spin-singlet Cooper pairs to enter, single-Cooper-pair tunneling is forbidden. But the product of two spin-triplet Cooper pairs has the component of total spin angular momentum $S_{\text{tot}} = 0$ that can enter the s-wave superconductor. In general, even number spin-triplet Cooper pairs have the component of total spin angular momentum $S_{\text{tot}} = 0$ but odd number spin-triplet Cooper pairs do not [71,72]. Therefore, with $\delta Q \cdot L = \pi/2$, the SC/Sm/SC junction only allows the tunneling of even number Cooper pairs, which should eliminate all the Josephson potential terms with odd times $\hat{\phi}$. To confirm this result, we build a tight-binding (TB) model Bogoliubov–de Gennes Hamiltonian of the SC/Sm/SC junction [71]. In the following calculation, We take $g = 26$ [73] and $\tilde{\alpha} k_f \gg g\mu_B B$ with k_f the Fermi wave vector in the semiconductor region and $\Delta/h = 45$ GHz [74] with Δ the superconducting gap. We obtain the Josephson potentials through three steps: We first calculate the eigenenergies of this TB Hamiltonian as a function of superconducting phase difference ϕ and B; we then sum all negative eigenenergies to get the zero temperature free energy, $F(\phi, B)$, of the junction; last, we perform the Fourier transform of $\cos(m\phi)$ and $\sin(m\phi)$ with m up to 20 to obtain the corresponding $E_{J\alpha}^m(B)$ and $E_{J\beta}^m(B)$.

Due to the high transparency of the SC/Sm/SC junction, we only need several transverse channels in the normal region to have strong enough Josephson potential strength. For simplicity, we first consider one channel with the chemical potential indicated by the blue dashed lines in Fig. 2(a). The magnitudes of the leading Josephson potential $E_{J\alpha}^{(m=1,2,3)}(B)$ and $E_{J\beta}^{(m=1)}(B)$ are plotted in Fig. 2(b), which come from the Fourier components of the free energy as discussed in the last paragraph. We found that $E_{J\beta}^{(m)} \approx 0$ in all considered magnetic field ranges and all the $E_\alpha^{(2m+1)}$ vanish simultaneously at a certain B [blue dashed lines in the inset of Fig. 2(b), which is consistent to our spin angular momentum analysis of the Cooper pairs.
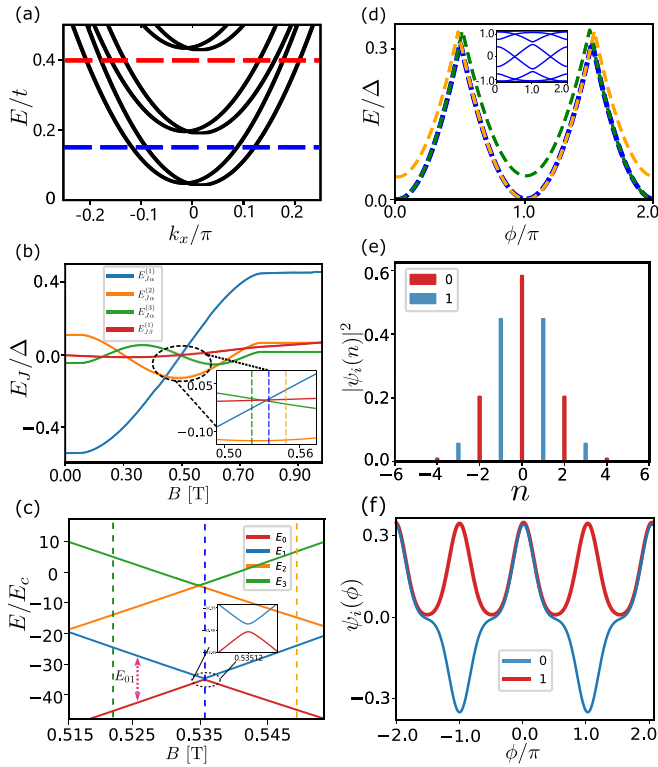
FIG. 2. (a) Energy band with periodic condition in the x direction. (b) Several leading terms of the Josephson potential vary with the magnetic field. The inset is around the 0-π transition. (c) Four lowest eigenenergies vary with the magnetic field around the 0-π transition. (d) Free energies' shape as a function of ϕ with three magnetic field magnitudes, corresponding to three vertical lines in (c). The inset is the ABS at 0-π point. (e) Charge distribution and (f) phase distribution of the two lowest states. All plots are under the condition $E_{j\alpha}^{(2)}/E_c \approx 50$ and $n_g = 0$.

With these Josephson potentials, we write the qubit Hamiltonian in the Cooper pair number basis [75,76],

$$H = \sum_{nn'm} \left(4E_c(n - n_g)^2 \delta_{n,n'} + E_J^m \delta_{n,n'+m} \right)|n\rangle\langle n'|$$
$$+ \text{H.c.}, \tag{5}$$

with E_c the charging energy, n and n' the Cooper pair numbers, n_g the offset charge, and $E_J^m = (E_{J\alpha}^{(m)} + iE_{J\beta}^{(m)})/2$ the mth nearest hopping due to the m Cooper pairs tunneling simultaneously. Figure 2(c) shows the lowest four eigenenergies with finite E_c and $n_g = 0$ as a function of magnetization. When the lowest two energies become almost degenerate [blue dashed lines in Fig. 2(c)], the Josephson junction is at the 0- to π-junction transition point, reflected in the degenerated double-well potential of the free energy and the π-periodic Andreev levels [Fig. 2(d)]. Notice that, at the transition point, the two lowest energy states do not completely degenerate but have a finite energy gap proportional to E_c [inset of Fig. 2(c)]. We plot the probability distribution of these two states in both Cooper pair number ($\hat{n}$) basis [Fig. 2(e)] and phase ($\hat{\phi}$) basis [Fig. 2(f)]. In the $\hat{n}$ axis, the two wave functions $|\psi_0\rangle$ and $|\psi_1\rangle$ are the eigenstates of the Cooper pair parity operator $\hat{P} = e^{i\hat{n}\pi}$ with eigenvalues $+1$ and -1, respectively. In the ϕ basis, each
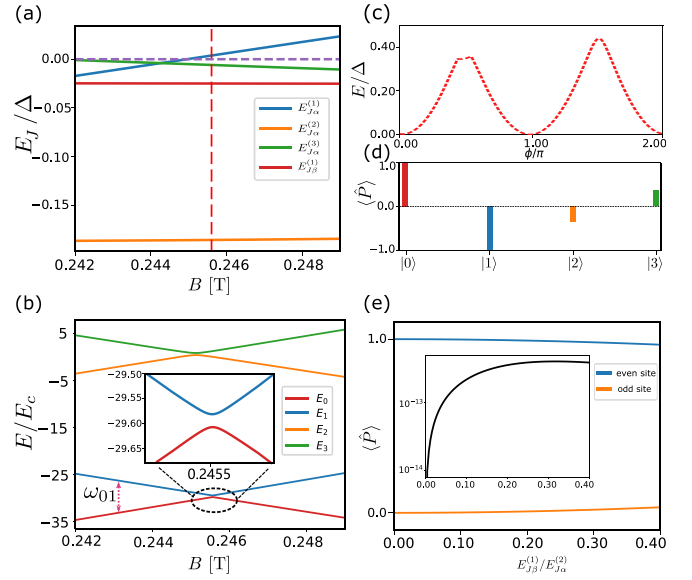

FIG. 3. Two channels with Dresselhaus SOC $\beta = 0.2\alpha$. (a) Several leading terms of the Josephson potential. (b) The energy levels vary with the magnetic field around the 0-π transition point. (c) Free energy at the 0-π transition point. (d) Cooper pair parity expectation values of the lowest four states. (e) The lowest energy state distribution on an even site and an odd site as a function of $E_{J\beta}^{(1)}/E_{J\alpha}^{(2)}$ with the condition $n_g = 0$, and $E_{J\alpha}^{(2)}/E_c \approx 50$; the inset is the logarithmic plot of the matrix element $\langle\psi_0|E_{J\beta}^{(1)}\sin\hat{\phi}|\psi_1\rangle/E_{01}$.

eigenstate is mainly distributed around $\phi = 0$ and $\phi = \pi$ with the property

$$|\psi_{0(1)}\rangle = \frac{|\phi \approx 0\rangle + (-)|\phi \approx \pi\rangle}{\sqrt{2}}, \tag{6}$$

where $|\phi \approx 0\rangle$ and $|\phi \approx \pi\rangle$ refer to the state solely localized at the potential wells $\phi = 0$ and $\phi = \pi$ [Fig. 2(d)], respectively. Therefore, we obtain a nearly degenerated qubit [Fig. 2(c)], which has an energy splitting around E_c and is isolated from other states by an energy gap around $\sqrt{32E_{j\alpha}^{(2)}E_c}$ [8].

In reality, the semiconductor may have multiple channels and finite Dresselhaus SOC. We increase the chemical potential to have two transverse channels at the Fermi level [Fig. 2(a)] and add Dresselhaus SOC with $\beta = 0.2\alpha$. Following the same Fourier transform procedures, we obtain the Josephson potential magnitudes $E_{J\alpha}^m$ and $E_{J\beta}^m$ and plot the leading terms in Fig. 3(a) around the transition point. We get finite $\sin\phi$ Josephson potential because the Zeeman effect and SOCs break the time-reversal and inversion symmetries, respectively. At $n_g = 0$, we consider the Josephson potentials up to $m = 20$ and plot the lowest four eigenenergies as a function of the magnetic field in Fig. 3(b). At the transition point [red dashed line in Figs. 3(a) and 3(b)], although the finite $\sin\phi$ Josephson potential changes the double-well potential shape significantly [Fig. 3(c)], the minima of the two potential wells locate around $\phi = 0$ and $\phi = \pi$ and remain
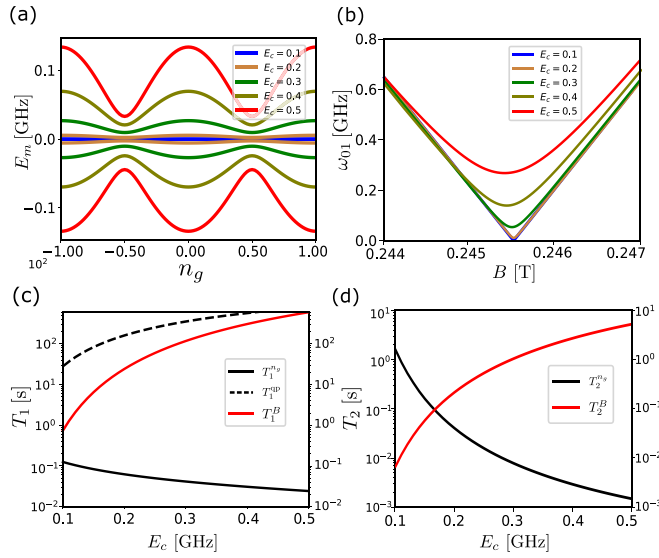
FIG. 4. Parameters are the same as in Fig. 3. (a) Qubit states' energies vary with n_g at the 0-π transition with different E_c. (b) ω_{01} varies with magnetic field around the 0-π transition point with different E_c. (c) and (d) T_1 and T_2 vary with E_c.

the same value. Therefore, the two lowest energy states at the transition point are still the Cooper pair parity eigenstates [Fig. 3(d)], reflecting on their Cooper pair parity expectation values ± 1 [Fig. 3(d)]. As a result, the qubit states with the potential in Fig. 3(c) at $n_g = 0$ can still be well described by Eq. (6). The lowest energy wave function only stays in the even number sites for $E_{J\beta}^{(1)}/E_{J\alpha}^{(2)}$ up to 0.4 [Fig. 3(e)] and the coupling between even and odd states through $\sin(\hat{\phi})$ potential is zero (inset of Fig. 3(e) [71]). Therefore our proposal is robust against imperfect fabrications.

Coherence properties of the 0-π qubit. To obtain the relaxation time of our 0-π qubit, we consider three noises: charge noise, magnetic field noise, and quasiparticle poisoning. Noted that our 0-π qubit relies on the charge sweet spot [$n_g = 0$ in Fig. 4(a)] and magnetic field sweet spot [the minimum $\omega_{01} = (E_1 - E_0)/h$ in Fig. 4(b)]. We thus expand the Hamiltonian up to the second order at the sweet spot as

$$H = H_0 + \frac{\partial H}{\partial \lambda}\delta\lambda(t) + \frac{1}{2}\frac{\partial^2 H}{\partial \lambda^2}\delta\lambda^2(t), \tag{7}$$

where H_0 is the Hamiltonian at $n_g = 0$ with the well potential shown in Fig. 3(b), and λ represents either charge (n_g) or magnetic field (B).

According to Fermi's golden rule [77], we can get T_1 from the inverse of the transition rate from initial state $|\psi_i\rangle$ to final state $|\psi_f\rangle$:

$$\Gamma_{i\to f} = \left|\left\langle\psi_f\left|\frac{\partial H}{\partial \lambda}\right|\psi_i\right\rangle\right|^2 S_\lambda(\omega_{fi}), \tag{8}$$

where $S_\lambda(\omega)$ is the noise power spectrum with an approximate $1/f$ spectrum, $S_\lambda(\omega) = 2\pi A_\lambda/|\omega|$ ($\omega_{ir} < \omega < \omega_{uv}$) [78,79]. Here we estimate that $\omega_{ir}/2\pi = 1$ Hz, $\omega_{uv}/2\pi = 0.4$ GHz which is determined by temperature ($T_m < 20$ mK),

$A_{n_g} = 10^{-8}\,e^2$ [8], $A_B = 10^{-17}$ T^2 [80] for charge and magnetic field noise, respectively. For charge noise, we have $\frac{\partial H}{\partial n_g}|_{n_g=0} = 8E_c\hat{n}\delta n_g$. As the two 0-$\pi$ qubit states are the eigenstates of Cooper pair parity operator $\hat{P}$, the qubit ordinary relaxation $\langle 0|\hat{n}|1\rangle$ vanishes. Therefore, the relaxation rate for charge noise is mainly from the depolarization rate [81–83],

$$\Gamma_1^{n_g} = \Gamma_{0\to 2}^{n_g} + \Gamma_{0\to 3}^{n_g} + \Gamma_{1\to 2}^{n_g} + \Gamma_{1\to 3}^{n_g}, \tag{9}$$

which describes the transition speed from qubit states, $|0\rangle$ and $|1\rangle$, to higher levels $|2\rangle$ and $|3\rangle$. The magnetic field noise is given by

$$\frac{\partial H}{\partial B} = \sum_m \frac{\partial E_{J\alpha}^{(m)}}{\partial B}\cos(m\phi) + \frac{\partial E_{J\beta}^{(m)}}{\partial B}\sin(m\phi),$$

which cause ordinary relaxation with the transition rate $\Gamma_1^B = |\langle 1|\frac{\partial H}{\partial B}|0\rangle|^2 S_B(\omega_{01})$. The associated relaxation times $T_1^{n_g}$ and T_1^B are plotted as the black and red solid curves in Fig. 4(c) respectively.

The quasiparticle poisoning comes from the fermionic quasiparticle tunneling through the Josephson junction [84] and is also a significant source of decoherence. In the traditional superconductor/insulator/superconductor junction, the quasiparticle obtains either $\phi/2$ or $-\phi/2$ phase after tunneling across the junction, which leads to the tunneling Hamiltonian

$$H_T = \tilde{t}\sum_{\eta,\kappa,\sigma} i\sin\left(\frac{\hat{\phi}}{2}\right)C_{\eta,\sigma}^{L\dagger}C_{\kappa,\sigma}^R + \text{H.c.}, \tag{10}$$

where $C_{\eta,\sigma}^{L(R)\dagger}$ ($C_{\eta,\sigma}^{L(R)}$) are quasiparticle creation (annihilation) operators on the left (right) lead and $\sigma = \uparrow, \downarrow$ accounts for spin; η, κ are the normal state indexes of leads. In our case, the Fermi surface splits due to the SOC and Zeeman field and brings the spin-dependent phase into the tunneling process. When there is only SOC, the electron and hole components have the same momentum due to the time-reversal symmetry [Fig. 5(a)]. The Zeeman field further shifts the electron and hole momenta to the opposite direction by $\pm\delta Q/2$ [Fig. 5(b)]. Note that this momentum shift is also the key to having finite center-of-mass momentum $\pm\delta Q$ of the Cooper pairs. When quasiparticles tunnel across the junction, they will carry the phase $\pm\delta Q \cdot L/2$ caused by the momentum shift in addition to the flux phase $\pm\phi/2$. The quasiparticle tunneling Hamiltonian takes the form

$$H_T = \sum_{\eta,\kappa,\sigma}\left[\tilde{t}_1 i\sin\left(\frac{\hat{\phi}}{2} + \frac{1}{2}\delta Q \cdot L\right)C_{\eta,\uparrow}^{L\dagger}C_{m\kappa,\uparrow}^R \right.$$
$$\left. + \tilde{t}_2 i\sin\left(\frac{\hat{\phi}}{2} - \frac{1}{2}\delta Q \cdot L\right)C_{\eta,\downarrow}^{L\dagger}C_{\kappa,\downarrow}^R\right] + \text{H.c.}, \tag{11}$$

where $\tilde{t}_{1(2)}$ are the tunneling amplitudes of the inner and outer Fermi surfaces [Fig. 5(a)] [71]. Accordingly, the transition elements due to quasiparticle poisoning take the form

$$\Gamma_{0\to 1} = \left|\langle 1|\sin\left(\frac{\hat{\phi}}{2} \pm \frac{1}{2}\delta Q \cdot L\right)|0\rangle\right|^2 S_{qp}(\omega_{01}). \tag{12}$$
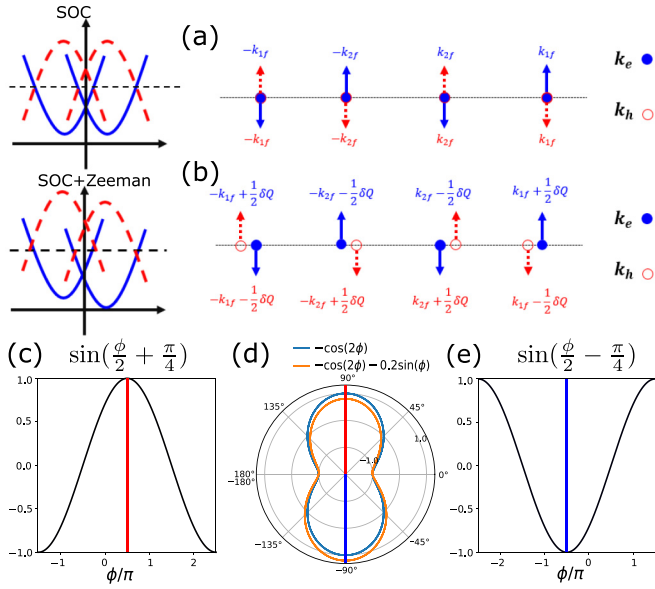
FIG. 5. (a) One-dimensional (1D) band dispersion and momenta at the Fermi surface with only SOC. (b) 1D band dispersion and momenta with only SOC and Zeeman splitting. The blue solid and red dashed lines indicate electron and hole respectively. The arrows represent the spin direction. (c) The quasiparticle tunneling Hamiltonian $\sin(\frac{\phi}{2} + \frac{\pi}{4})$ at the 0-π point. (d) The Josephson potentials in the polar angle, which naturally present the periodic boundary condition $\pi = -\pi$ of the ϕ axis. The red and blue lines correspond to $\phi = \pi/2$ and $\phi = -\pi/2$. (e) The quasiparticle tunneling Hamiltonian $\sin(\frac{\phi}{2} - \frac{\pi}{4})$ at the 0-π point.

The quasiparticle spectral density $S_{qp}(\omega) = \frac{\omega}{\pi g_K}\text{Re}[Y_{qp}(\omega)] = \frac{\omega}{\pi g_K}\frac{1}{2}\chi_{qp}g_T(\frac{2\Delta}{\omega})^{\frac{3}{2}}$, with g_K the conductance quantum, g_T the junction conductance, Δ the superconducting gap and χ_{qp} the quasiparticle density normalized to the Cooper-pair density that we take as 10^{-7} [85]. Note that at the 0-π transition point, $\sin(\frac{\hat{\phi}}{2} \pm \frac{1}{2}\delta Q \cdot L) = \sin(\frac{\hat{\phi}}{2} \pm \frac{\pi}{4})$ which is symmetric around $\phi = \pm\pi/2$ [Figs. 5(c) and 5(e)]. Because the $\phi = \pi$ and $\phi = -\pi$ correspond to the same point in the ϕ axis, we further plot the Josephson potential in the polar angle coordinate in Fig. 5(d), which clearly shows that the Josephson potential at the $0 - \pi$ transition point is also symmetric around $\phi = \pm\pi/2$. Note that this results holds even in the presence of $\sin\phi$ potential. Therefore the qubit states are the even and odd functions around $\phi = \pm\pi/2$ that cannot be flipped by the tunneling Hamiltonian proportional to $\sin(\frac{\hat{\phi}}{2} \pm \frac{\pi}{4})$. This means the quasiparticle poisoning is suppressed in our proposal. This conclusion is similar to that in the 0-π qubit with multiple Josephson junctions [21] and the fluxonium qubit [85] but due to a different mechanism. In reality, the $\delta Q \cdot L$ may not be exactly $\pi/2$, limited by the magnetic field accuracy. We take the magnetic field to deviate from the exact transition point by 1 G so that $\delta Q \cdot L = \pi/2 + \delta\theta$ with $\delta\theta \approx 2 \times 10^{-4}\pi$. The transition matrix element takes $\langle 0| \sin(\frac{\hat{\phi}}{2} + \frac{\pi}{4} \pm 10^{-4}\pi)|1\rangle$. To calculate this matrix element, we expand the potential at the minima of the two potential wells

$\phi = 0, \pi$,

$$H \approx 4E_c n^2 - 2E_{J\alpha}^{(2)}\hat{\phi}^2, \quad (13)$$

whose eigenfunction takes the form

$$\psi_l(\phi) = \left(\frac{\zeta}{2^l l! \sqrt{\pi}}\right)^{\frac{1}{2}} e^{-\frac{(\zeta\phi)^2}{2}} H_l(\zeta\phi), \quad (14)$$

with $\zeta \equiv (\frac{E_{J\alpha}^{(2)}}{2E_c})^{1/4}$, l the energy level index, and $H_l(x)$ the Hermite polynomials. The wave function in the other well π can be gained by shifting ϕ to $\phi - \pi$ so the qubit states $|0\rangle$ ($|1\rangle$) $= \frac{1}{\sqrt{2}}[\psi_{l=0}(\phi) + (-)\psi_{l=0}(\phi - \pi)]$. We then calculate the matrix element of Eq. (12) by integrating the product of the three components and plot T_1^{qp} as a function of E_c [black dashed curves in Fig. 4(c)], We find that T_1 is mainly limited by charge noise and takes $T_1 = 77$ ms for $E_c = 0.16$ GHz [Fig. 4(c)].

The dephasing time T_2 is related to the decay of off-diagonal term of the density matrix [8],

$$\rho_{01} = \exp\left(-iD_1\int_0^t \delta\lambda(t)dt - i\frac{1}{2}D_2\int_0^t \delta\lambda(t)^2 dt\right), \quad (15)$$

with $D_1 = \frac{\partial\omega_{01}}{\partial\lambda}$ and $D_2 = \frac{\partial^2\omega_{01}}{\partial\lambda^2}$. In our system, we take ω_{01} at the charge and magnetic field sweet spots so the linear noise susceptibility $D_1 = 0$. After a standard calculation [78,82], we have

$$T_2 = \left[D_2^2 A_\lambda^2 \ln^2\left(\frac{\omega_{uv}}{\omega_{ir}}\right) + 2D_2^2 A_\lambda^2 \ln^2\left(\frac{1}{\omega_{ir}t}\right)\right]^{-\frac{1}{2}}. \quad (16)$$

The second-order derivative $\partial^2\omega_{01}/\partial n_g^2$ increases with increasing the charge energy E_c [Fig. 4(a)]. Meanwhile, The second-order derivative $\partial^2\omega_{01}/\partial B^2$ decreases with increasing charge energy E_c [Fig. 4(b)] [71]. Therefore, increasing E_c, we get smaller $T_2^{n_g}$ but larger T_2^B as shown in Fig. 4(d). We estimate the dephasing time to be about $T_2 = 55$ ms at the crossing point $E_c \approx 0.16$ GHz [Fig 4(d)]. The control [14,20] and readout [20,21,23,66] of the 0-π qubit have been developed and can be applied to our proposal.

Conclusions. We propose to implement the 0-π qubit with one SC/Sm/SC Josephson junction. The internal spin degree of freedom of electrons in semiconductors naturally provides the two interference paths of Cooper pairs with similar transport parameters such as transmission amplitude. The qubit states are the eigenstates of the Cooper pair parity operator and are nearly degenerate. These properties are robust against various deviations from the ideal model and dramatically increase the qubit relaxation time T_1 and coherent time T_2. The multidimensionally tunable SC/Sm/SC junction is a promising platform to realize a parity-protected 0-π qubit.

[1] Y. Makhlin, G. Schön, and A. Shnirman, Rev. Mod. Phys. **73**, 357 (2001).

[2] J. Q. You and F. Nori, Phys. Today **58**(11), 42 (2005).

[3] F. Arute, K. Arya, R. Babbush, D. Bacon, J. C. Bardin, R. Barends, R. Biswas, S. Boixo, F. G. S. L. Brandao, D. A. Buell, B. Burkett, Y. Chen, Z. Chen, B. Chiaro, R. Collins, W. Courtney, A. Dunsworth, E. Farhi, B. Foxen, A. Fowler *et al.*, Nature (London) **574**, 505 (2019).

[4] Y. Wu, W.-S. Bao, S. Cao, F. Chen, M.-C. Chen, X. Chen, T.-H. Chung, H. Deng, Y. Du, D. Fan, M. Gong, C. Guo, C. Guo, S. Guo, L. Han, L. Hong, H.-L. Huang, Y.-H. Huo, L. Li, N. Li *et al.*, Phys. Rev. Lett. **127**, 180501 (2021).

[5] B. Josephson, Phys. Lett. **1**, 251 (1962).

[6] P. W. Anderson and J. M. Rowell, Phys. Rev. Lett. **10**, 230 (1963).

[7] M. H. Devoret, A. Wallraff, and J. M. Martinis, arXiv:cond-mat/0411174.

[8] J. Koch, T. M. Yu, J. Gambetta, A. A. Houck, D. I. Schuster, J. Majer, A. Blais, M. H. Devoret, S. M. Girvin, and R. J. Schoelkopf, Phys. Rev. A **76**, 042319 (2007).

[9] H. Paik, D. I. Schuster, L. S. Bishop, G. Kirchmair, G. Catelani, A. P. Sears, B. R. Johnson, M. J. Reagor, L. Frunzio, L. I. Glazman, S. M. Girvin, M. H. Devoret, and R. J. Schoelkopf, Phys. Rev. Lett. **107**, 240501 (2011).

[10] R. Barends, J. Kelly, A. Megrant, D. Sank, E. Jeffrey, Y. Chen, Y. Yin, B. Chiaro, J. Mutus, C. Neill, P. O'Malley, P. Roushan, J. Wenner, T. C. White, A. N. Cleland, and J. M. Martinis, Phys. Rev. Lett. **111**, 080502 (2013).

[11] L. Casparis, T. W. Larsen, M. S. Olsen, F. Kuemmeth, P. Krogstrup, J. Nygård, K. D. Petersson, and C. M. Marcus, Phys. Rev. Lett. **116**, 150505 (2016).

[12] A. P. M. Place, L. V. H. Rodgers, P. Mundada, B. M. Smitham, M. Fitzpatrick, Z. Leng, A. Premkumar, J. Bryon, A. Vrajitoarea, S. Sussman, G. Cheng, T. Madhavan, H. K. Babla, X. H. Le, Y. Gang, B. Jäck, A. Gyenis, N. Yao, R. J. Cava, N. P. de Leon *et al.*, Nat. Commun. **12**, 1779 (2021).

[13] A. Kitaev, arXiv:cond-mat/0609441.

[14] P. Brooks, A. Kitaev, and J. Preskill, Phys. Rev. A **87**, 052306 (2013).

[15] B. Douçot and J. Vidal, Phys. Rev. Lett. **88**, 227005 (2002).

[16] C. Benjamin and J. K. Pachos, Phys. Rev. B **79**, 155431 (2009).

[17] M. T. Bell, J. Paramanandam, L. B. Ioffe, and M. E. Gershenson, Phys. Rev. Lett. **112**, 167001 (2014).

[18] M. Rymarz, S. Bosco, A. Ciani, and D. P. DiVincenzo, Phys. Rev. X **11**, 011032 (2021).

[19] J. M. Dempster, B. Fu, D. G. Ferguson, D. I. Schuster, and J. Koch, Phys. Rev. B **90**, 094518 (2014).

[20] A. D. Paolo, A. L. Grimsmo, P. Groszkowski, J. Koch, and A. Blais, New J. Phys. **21**, 043002 (2019).

[21] W. C. Smith, A. Kou, X. Xiao, U. Vool, and M. H. Devoret, npj Quantum Inf. **6**, 8 (2020).

[22] K. Kalashnikov, W. T. Hsieh, W. Zhang, W.-S. Lu, P. Kamenov, A. Di Paolo, A. Blais, M. E. Gershenson, and M. Bell, PRX Quantum **1**, 010307 (2020).

[23] A. Gyenis, P. S. Mundada, A. Di Paolo, T. M. Hazard, X. You, D. I. Schuster, J. Koch, A. Blais, and A. A. Houck, PRX Quantum **2**, 010339 (2021).

[24] T. Schäpers, *Superconductor/Semiconductor Junctions*, Springer Tracts in Modern Physics (Springer, Berlin, 2001).

[25] X. Blase, E. Bustarret, C. Chapelier, T. Klein, and C. Marcenat, Nat. Mater. **8**, 375 (2009).

[26] H. Y. Günel, I. E. Batov, H. Hardtdegen, K. Sladek, A. Winden, K. Weis, G. Panaitov, D. Grützmacher, and T. Schäpers, J. Appl. Phys. **112**, 034316 (2012).

[27] S. V. Mironov, A. S. Mel'nikov, and A. I. Buzdin, Phys. Rev. Lett. **114**, 227001 (2015).

[28] H. J. Suominen, J. Danon, M. Kjaergaard, K. Flensberg, J. Shabani, C. J. Palmstrøm, F. Nichele, and C. M. Marcus, Phys. Rev. B **95**, 035307 (2017).

[29] M. Kjaergaard, H. J. Suominen, M. P. Nowak, A. R. Akhmerov, J. Shabani, C. J. Palmstrøm, F. Nichele, and C. M. Marcus, Phys. Rev. Applied **7**, 034029 (2017).

[30] A. I. Buzdin, Rev. Mod. Phys. **77**, 935 (2005).

[31] F. S. Bergeret, A. F. Volkov, and K. B. Efetov, Rev. Mod. Phys. **77**, 1321 (2005).

[32] X. Liu, J. K. Jain, and C.-X. Liu, Phys. Rev. Lett. **113**, 227002 (2014).

[33] E. C. Gingrich, B. M. Niedzielski, J. A. Glick, Y. Wang, D. L. Miller, R. Loloee, W. P. Pratt Jr, and N. O. Birge, Nat. Phys. **12**, 564 (2016).

[34] D. B. Szombati, S. Nadj-Perge, D. Car, S. R. Plissard, E. P. A. M. Bakkers, and L. P. Kouwenhoven, Nat. Phys. **12**, 568 (2016).

[35] I. V. Bobkova, A. M. Bobkov, and M. A. Silaev, Phys. Rev. Lett. **127**, 147701 (2021).

[36] L. Fu and C. L. Kane, Phys. Rev. B **79**, 161408(R) (2009).

[37] D. M. Badiane, M. Houzet, and J. S. Meyer, Phys. Rev. Lett. **107**, 177002 (2011).

[38] F. Qu, F. Yang, J. Shen, Y. Ding, J. Chen, Z. Ji, G. Liu, J. Fan, X. Jing, C. Yang, and L. Lu, Sci. Rep. **2**, 339 (2012).

[39] J. R. Williams, A. J. Bestwick, P. Gallagher, S. S. Hong, Y. Cui, A. S. Bleich, J. G. Analytis, I. R. Fisher, and D. Goldhaber-Gordon, Phys. Rev. Lett. **109**, 056803 (2012).

[40] S. Cho, B. Dellabetta, A. Yang, J. Schneeloch, Z. Xu, T. Valla, G. Gu, M. J. Gilbert, and N. Mason, Nat. Commun. **4**, 1689 (2013).

[41] J. B. Oostinga, L. Maier, P. Schüffelgen, D. Knott, C. Ames, C. Brüne, G. Tkachov, H. Buhmann, and L. W. Molenkamp, Phys. Rev. X **3**, 021007 (2013).

[42] I. Sochnikov, L. Maier, C. A. Watson, J. R. Kirtley, C. Gould, G. Tkachov, E. M. Hankiewicz, C. Brüne, H. Buhmann, L. W. Molenkamp, and K. A. Moler, Phys. Rev. Lett. **114**, 066801 (2015).

[43] F. Dolcini, M. Houzet, and J. S. Meyer, Phys. Rev. B **92**, 035428 (2015).

[44] J. Wiedenmann, E. Bocquillon, R. S. Deacon, S. Hartinger, O. Herrmann, T. M. Klapwijk, L. Maier, C. Ames, C. Bruene, C. Gould, A. Oiwa, K. Ishibashi, S. Tarucha, H. Buhmann, and L. W. Molenkamp, Nat. Commun. **7**, 10303 (2016).

[45] E. Bocquillon, R. S. Deacon, J. Wiedenmann, P. Leubner, T. M. Klapwijk, C. Bruene, K. Ishibashi, H. Buhmann, and L. W. Molenkamp, Nat. Nanotechnol. **12**, 137 (2017).

[46] S. Gladchenko, D. Olaya, E. Dupont-Ferrier, B. Douot, L. B. Ioffe, and M. E. Gershenson, Nat. Phys. **5**, 48 (2009).

[47] M. Hays, G. de Lange, K. Serniak, D. J. van Woerkom, D. Bouman, P. Krogstrup, J. Nygård, A. Geresdi, and M. H. Devoret, Phys. Rev. Lett. **121**, 047001 (2018).

[48] J. I.-J. Wang, D. Rodan-Legrain, L. Bretheau, D. L. Campbell, B. Kannan, D. Kim, M. Kjaergaard, P. Krantz, G. O. Samach, F. Yan, J. L. Yoder, K. Watanabe, T. Taniguchi, T. P. Orlando, S. Gustavsson, P. Jarillo-Herrero, and W. D. Oliver, Nat. Nanotechnol. **14**, 120 (2019).

[49] A. Bargerbos, W. Uilhoorn, C.-K. Yang, P. Krogstrup, L. P. Kouwenhoven, G. de Lange, B. van Heck, and A. Kou, Phys. Rev. Lett. **124**, 246802 (2020).

[50] A. Kringhøj, B. van Heck, T. W. Larsen, O. Erlandsson, D. Sabonis, P. Krogstrup, L. Casparis, K. D. Petersson, and C. M. Marcus, Phys. Rev. Lett. **124**, 246803 (2020).

[51] M. Hays, V. Fatemi, K. Serniak, D. Bouman, S. Diamond, G. de Lange, P. Krogstrup, J. Nygård, A. Geresdi, and M. H. Devoret, Nat. Phys. **16**, 1103 (2020).

[52] M. Hays, V. Fatemi, D. Bouman, J. Cerrillo, S. Diamond, K. Serniak, T. Connolly, P. Krogstrup, J. Nygård, A. Levy Yeyati, A. Geresdi, and M. H. Devoret, Science **373**, 430 (2021).

[53] C. Baumgartner, L. Fuchs, L. Frész, S. Reinhardt, S. Gronin, G. C. Gardner, M. J. Manfra, N. Paradiso, and C. Strunk, Phys. Rev. Lett. **126**, 037001 (2021).

[54] T. W. Larsen, K. D. Petersson, F. Kuemmeth, T. S. Jespersen, P. Krogstrup, J. Nygård, and C. M. Marcus, Phys. Rev. Lett. **115**, 127001 (2015).

[55] G. de Lange, B. van Heck, A. Bruno, D. J. van Woerkom, A. Geresdi, S. R. Plissard, E. P. A. M. Bakkers, A. R. Akhmerov, and L. DiCarlo, Phys. Rev. Lett. **115**, 127002 (2015).

[56] L. Casparis, M. R. Connolly, M. Kjaergaard, N. J. Pearson, A. Kringhøj, T. W. Larsen, F. Kuemmeth, T. Wang, C. Thomas, S. Gronin, G. C. Gardner, M. J. Manfra, C. M. Marcus, and K. D. Petersson, Nat. Nanotechnol. **13**, 915 (2018).

[57] A. Kringhøj, L. Casparis, M. Hell, T. W. Larsen, F. Kuemmeth, M. Leijnse, K. Flensberg, P. Krogstrup, J. Nygård, K. D. Petersson, and C. M. Marcus, Phys. Rev. B **97**, 060508(R) (2018).

[58] L. Casparis, N. J. Pearson, A. Kringhøj, T. W. Larsen, F. Kuemmeth, J. Nygård, P. Krogstrup, K. D. Petersson, and C. M. Marcus, Phys. Rev. B **99**, 085434 (2019).

[59] A. Kringhøj, T. W. Larsen, B. van Heck, D. Sabonis, O. Erlandsson, I. Petkovic, D. I. Pikulin, P. Krogstrup, K. D. Petersson, and C. M. Marcus, Phys. Rev. Lett. **124**, 056801 (2020).

[60] D. Sabonis, O. Erlandsson, A. Kringhøj, B. van Heck, T. W. Larsen, I. Petkovic, P. Krogstrup, K. D. Petersson, and C. M. Marcus, Phys. Rev. Lett. **125**, 156804 (2020).

[61] S. A. Khan, C. Lampadaris, A. Cui, L. Stampfer, Y. Liu, S. J. Pauka, M. E. Cachaza, E. M. Fiordaliso, J.-H. Kang, S. Korneychuk, T. Mutas, J. E. Sestoft, F. Krizek, R. Tanta, M. C. Cassidy, T. S. Jespersen, and P. Krogstrup, arXiv:2003.04487.

[62] G. V. Graziano, J. S. Lee, M. Pendharkar, C. J. Palmstrøm, and V. S. Pribiag, Phys. Rev. B **101**, 054510 (2020).

[63] J. Linder and J. W. A. Robinson, Nat. Phys. **11**, 307 (2015).

[64] M. Hell, M. Leijnse, and K. Flensberg, Phys. Rev. Lett. **118**, 107701 (2017).

[65] Y. Volpez, D. Loss, and J. Klinovaja, Phys. Rev. Lett. **122**, 126402 (2019).

[66] T. W. Larsen, M. E. Gershenson, L. Casparis, A. Kringhøj, N. J. Pearson, R. P. G. McNeil, F. Kuemmeth, P. Krogstrup, K. D. Petersson, and C. M. Marcus, Phys. Rev. Lett. **125**, 056801 (2020).

[67] R. Winkler, *Spin-orbit Coupling Effects in Two-Dimensional Electron and Hole Systems* (Springer-Verlag, Berlin, 2003).

[68] F. Pientka, A. Keselman, E. Berg, A. Yacoby, A. Stern, and B. I. Halperin, Phys. Rev. X **7**, 021032 (2017).

[69] C. Li, B. de Ronde, J. de Boer, J. Ridderbos, F. Zwanenburg, Y. Huang, A. Golubov, and A. Brinkman, Phys. Rev. Lett. **123**, 026802 (2019).

[70] C. T. Ke, C. M. Moehle, F. K. de Vries, C. Thomas, S. Metti, C. R. Guinn, R. Kallaher, M. Lodari, G. Scappucci, T. Wang, R. E. Diaz, G. C. Gardner, M. J. Manfra, and S. Goswami, Nat. Commun. **10**, 3764 (2019).

[71] See Supplemental Material at http://link.aps.org/supplemental/10.1103/PhysRevB.105.L180502 for I. The Josephson coupling coefficients vary with magnetic field; II. The physical interpretation of and the explicit form for the high-order Josephson potentials; III. The effect of high-order Josephson coupling on E_{01}; IV. The analysis of the $\sin(\phi)$ effect on the qubit states; V. Quasiparticle poisoning; VI. Theoretical calculation of T_2.

[72] C. W. Groth, M. Wimmer, A. R. Akhmerov, and X. Waintal, New J. Phys. **16**, 063065 (2014).

[73] F. Qu, J. van Veen, F. K. de Vries, A. J. A. Beukman, M. Wimmer, W. Yi, A. A. Kiselev, B.-M. Nguyen, M. Sokolich, M. J. Manfra, F. Nichele, C. M. Marcus, and L. P. Kouwenhoven, Nano Lett. **16**, 7509 (2016).

[74] W. Chang, S. M. Albrecht, T. S. Jespersen, F. Kuemmeth, P. Krogstrup, J. Nygård, and C. M. Marcus, Nat. Nanotechnol. **10**, 232 (2015).

[75] V. Bouchiat, D. Vion, P. Joyez, D. Esteve, and M. H. Devoret, Phys. Scr. **T76**, 165 (1998).

[76] R. Alicki, arXiv:0911.3016.

[77] D. J. Griffiths, *Introduction to Quantum Mechanics* (Cambridge University Press, Cambridge, 2018).

[78] G. Ithier, E. Collin, P. Joyez, P. J. Meeson, D. Vion, D. Esteve, F. Chiarello, A. Shnirman, Y. Makhlin, J. Schriefl, and G. Schön, Phys. Rev. B **72**, 134519 (2005).

[79] E. Paladino, Y. M. Galperin, G. Falci, and B. L. Altshuler, Rev. Mod. Phys. **86**, 361 (2014).

[80] A. Blais, J. Gambetta, A. Wallraff, D. I. Schuster, S. M. Girvin, M. H. Devoret, and R. J. Schoelkopf, Phys. Rev. A **75**, 032329 (2007).

[81] A. A. Clerk, M. H. Devoret, S. M. Girvin, F. Marquardt, and R. J. Schoelkopf, Rev. Mod. Phys. **82**, 1155 (2010).

[82] P. Groszkowski, A. D. Paolo, A. L. Grimsmo, A. Blais, D. I. Schuster, A. A. Houck, and J. Koch, New J. Phys. **20**, 043053 (2018).

[83] P. Krantz, M. Kjaergaard, F. Yan, T. P. Orlando, S. Gustavsson, and W. D. Oliver, Appl. Phys. Rev. **6**, 021318 (2019).

[84] G. Catelani, R. J. Schoelkopf, M. H. Devoret, and L. I. Glazman, Phys. Rev. B **84**, 064517 (2011).

[85] I. M. Pop, K. Geerlings, G. Catelani, R. J. Schoelkopf, L. I. Glazman, and M. H. Devoret, Nature (London) **508**, 369 (2014).